Signatures of coherent vibrational energy transfer in IR and Raman line shapes for liquid water

Mino Yang[a] and J. L. Skinner[b]

Received 4th September 2009, Accepted 28th October 2009
First published as an Advance Article on the web 2nd December 2009
DOI: 10.1039/b918314k

We calculate theoretical IR and Raman line shapes for the OH stretch region of liquid water, using mixed quantum/classical and electronic-structure/molecular-dynamics methods. Our approach improves upon the time-averaging approximation used earlier for the same problem, and our results are in excellent agreement with experiment. Previous analysis of theoretical results for this problem considered the extent of delocalization (over local OH stretch excitations) of the instantaneous vibrational eigenstates. In this work we present a complementary analysis in the time-domain, by decomposing the appropriate response functions into diagonal and off-diagonal contributions (in the local mode basis). Our analysis indicates that all vibrational spectra show signatures of coherent vibrational energy transfer. This is manifest in different (IR, isotropic and depolarized Raman) experiments to different extents, because of the competition between coherent energy transfer and rotational disorder.

I. Introduction

Water, with its strong intermolecular hydrogen-bonding ability, is important in many areas of chemistry, biology, environmental sciences, and modern technology. Various vibrational spectroscopic techniques such as IR absorption,[1,2] Raman scattering,[2–6] pump–probe (IR–IR and IR-Raman),[7–9] hole-burning,[10] and coherent nonlinear IR spectroscopies[11–16] are valuable tools for understanding the structure and dynamics of water. Vibrational spectroscopies probing OH stretching modes are particularly useful because transition frequencies are sensitive to local molecular environments.[17] Theoretical studies have also provided valuable information about the structure and dynamics of liquid water.[17–28] Many theoretical[20,23,26–28] and experimental[6,10–12,14,29,30] studies have been performed on the HOD impurity in water or heavy water in order to explore structure and dynamics. For example, in the latter case, the OH stretching mode of HOD may be regarded as an isolated chromophore, since the transition energy of the OH stretching mode is off-resonant with other modes in the system. Thus, one may obtain useful information about solvent dynamics in the absence of the complexity resulting from molecular couplings.

In spite of the valuable information obtained from these isotopic studies, it is still desirable to perform spectroscopic experiments on pure water,[1,7,8,13,16,21,31–33] which is a real solvent in many important applications. Moreover, the rich vibrational dynamics of this complicated excitonic system is of significant interest. Although state-of-the-art time-domain techniques using coherent lasers provide us with direct information about dynamics, their theoretical modeling is demanding because of the doubly excited states.[33,34] The most fundamental experiments, IR absorption and incoherent Raman line shapes, which are free from these complications due to double excitations, can also be powerful tools for analyzing the structure and dynamics of water when they are combined with theoretical models. In comparison with spectra of the isotope impurity, the spectra of water reveal several interesting features: (1) the water IR spectrum is broader, (2) IR absorption and polarized Raman spectra show the appearance of side bands on the red side, (3) isotropic and anisotropic Raman line shapes are different.

In order to calculate the vibrational spectra of modes with high frequencies, a quantum-mechanical description of the modes is required. Mixed quantum/classical (QM/CM) methods to calculate the line shapes of OH stretching modes in water have been recently reported by a few groups.[11,19–21,28,31,35–37] They differ mainly in the mapping relations for the fluctuations of the Hamiltonian and the number of adjustable parameters employed. Among them, the method developed by the Skinner group has no adjustable parameters, and all the microscopic variables have been determined *a priori* by electronic structure calculations based on quantum-mechanical density functional theory.[28,36,38] The influence of other degrees of freedom with lower characteristic frequencies on the quantum-mechanical Hamiltonian was treated by classical molecular dynamics simulation with the SPC/E water model.[39] Using the QM/CM method, the theoretical line shapes are in reasonably good agreement with experimental spectra.[36]

All the interesting spectral features mentioned above were qualitatively reproduced by the theory,[36] and turned out to originate from the delocalized nature of the excited vibrational states produced by intramolecular and dipole–dipole couplings between the modes. Even though the

[a] *Department of Chemistry and Basic Sciences Research Institute, Chungbuk National University, Cheongju, Chungbuk 361-763, Republic of KoreaDepartment of Chemistry and Theoretical Chemistry Institute, University of Wisconsin, on sabbatical visit at UW-Madison, Madison WI 53706. E-mail: MinoYang@chungbuk.ac.kr*
[b] *Department of Chemistry and Theoretical Chemistry Institute, University of Wisconsin, Madison WI 53706. E-mail: skinner@chem.wisc.edu*

magnitudes of the couplings are much smaller than the total width of the frequency distribution, Auer and Skinner found that the excited states of many OH stretching modes are delocalized over up to ten OH chromophores.[36] It was shown that the delocalized nature of the excited states has a large impact on the experimentally-observed spectral patterns, and therefore they claimed that traditional assignments of spectral peaks to different molecular environments[1,5,40,41] or to symmetric and antisymmetric normal modes of water molecules[42] might be erroneous. Due to computational expense, however, an approximate method, called the time-averaging approximation,[43] was introduced in their study to incorporate the effects of dynamical fluctuations of diagonal and off-diagonal Hamiltonian matrix elements. Moreover, the spectral analysis was performed by looking at instantaneous eigenstates, which would only be strictly appropriate if the system were in the inhomogenous (static) limit. It is, therefore, desirable to examine how an exact treatment of dynamical fluctuations[31,44] affects the spectral shapes, in comparison with the approximate results and with experimental data.

In this paper, employing the QM/CM method developed by Auer and Skinner, we remove the time-averaging approximation, thus solving the line shape problem exactly. We find, in fact, that the time-averaging approximation works very well. By analyzing the line shapes in the time domain, in terms of diagonal and off-diagonal response functions, we show that spectral features can be interpreted in terms of coherent vibrational energy transfer dynamics, complementing the frequency-domain interpretation of Auer and Skinner. This time-domain analysis, which takes into account all dynamics exactly, also removes any worries about the appropriateness of our previous analysis,[36] which is only strictly valid in the static limit.[43] In any case, we confirm that a collective band is created by this coherent excitation dynamics, and show how the band is manifested, to different extents, in IR absorption, and isotropic and polarized Raman spectroscopies. In particular, the differences among the line shapes result from the scalar, vector, and tensor nature of the field-matter interactions for isotropic Raman, IR absorption, and depolarized Raman line shapes, respectively.

II. IR and Raman line shapes

Utilizing the time-correlation function formalism, IR absorption and Raman line shapes are given by[45]

$$I(\omega) = 2\mathrm{Re}\int_0^\infty \mathrm{d}t e^{i\omega t}\phi(t) \tag{1}$$

where $\phi(t)$, called a response function, is a time-correlation function of a quantum-mechanical operator relevant to each experiment. These time-domain expressions for the IR and Raman spectroscopies are advantageous both for line shape calculations, and for their interpretation in terms of dynamical processes of the system.

In absorption spectroscopy, incident light interacts with a system *via* its transition dipoles, and the response function for an *isotropic* sample such as a liquid is given by the dipole–dipole time-correlation function:

$$\phi_{\mathrm{IR}}(t) = \tfrac{1}{3}\langle\vec{\mu}(t)\cdot\vec{\mu}(0)\rangle \tag{2}$$

where $\vec{\mu}(t)$ is the Heisenberg representation for the dipole vector of the system at time t and $\langle\cdot\cdot\rangle$ indicates the ensemble average over the equilibrium density matrix.

In Raman spectroscopies, off-resonant incident light induces transient dipoles in the system proportional to its molecular polarizabilities, and the induced dipoles emit scattered light. In this case, the response functions are given by the time-correlation functions of the polarizability tensor, $\underline{\underline{\alpha}}$, which can be decomposed into two parts,

$$\underline{\underline{\alpha}} = \bar{\alpha}\underline{\underline{I}} + \underline{\underline{\beta}} \tag{3}$$

where $\bar{\alpha} \equiv \frac{1}{3}\mathrm{Tr}(\underline{\underline{\alpha}})$ is the isotropic component of $\underline{\underline{\alpha}}$, and $\underline{\underline{\beta}}$ is the remaining anisotropic polarizability. $\underline{\underline{I}}$ is the unit tensor and Tr denotes a trace over three-dimensional space. The contributions of those two components to the Raman line shape depend on detailed configurations of experiments. Conventional Raman spectroscopies are often performed with linearly-polarized incident light. Light scattered perpendicular to the incident light is collected, and often is filtered by a polarizer. When the filtered light has a polarization perpendicular to that of the incident light, this is referred to as the VH (perpendicular-polarized) Raman spectroscopy. When the polarization of the filtered light is parallel to that of the incident light, this is referred to as the VV (parallel-polarized) Raman spectroscopy. The response functions in an *isotropic* sample, which are averaged over all (orthogonal) directions of incident and scattered light, are expressed in terms of the time-correlation functions of the isotropic and anisotropic polarizabilities:[45]

$$\phi_{\mathrm{VH}}(t) = \frac{1}{10}\Delta_{\mathrm{aniso}}(t) \tag{4}$$

$$\phi_{\mathrm{VV}}(t) = \Delta_{\mathrm{iso}}(t) + \frac{2}{15}\Delta_{\mathrm{aniso}}(t) \tag{5}$$

where $\Delta_{\mathrm{aniso}}(t) \equiv \langle\mathrm{Tr}(\underline{\underline{\beta}}(t)\cdot\underline{\underline{\beta}}(0))\rangle$ and $\Delta_{\mathrm{iso}}(t)\equiv\langle\bar{\alpha}(t)\bar{\alpha}(0)\rangle$. $\bar{\alpha}(t)$ and $\underline{\underline{\beta}}(t)$ are, respectively, the Heisenberg representation for each operator at time t. The isotropic Raman line shape is obtained by a linear combination of the two measurable Raman line shapes, $I_{\mathrm{iso}}(\omega) = I_{\mathrm{VV}}(\omega) - \frac{4}{3}I_{\mathrm{VH}}(\omega)$, so that the response function for it involves only the time-correlation function of the *isotropic* polarizability:

$$\phi_{\mathrm{iso}}(t) = \phi_{\mathrm{VV}}(t) - \frac{4}{3}\phi_{\mathrm{VH}}(t) = \Delta_{\mathrm{iso}}(t). \tag{6}$$

Since the VH Raman spectrum is determined by the time-correlation function of the anisotropic polarizability (eqn (4)), VH Raman experiments are often called anisotropic Raman experiments.

III. Mixed quantum/classical approach

In order to obtain the theoretical line shapes, one needs to calculate the time evolution of the dipole vector and polarizability tensor. For this, the QM/CM approach is employed. An application of this approach for the IR and Raman line shapes of water has been developed by Auer and Skinner[26,36] and is summarized here. The hindered-translational and librational degrees of freedom (called the bath) of the water molecules are approximately described by

classical mechanics with a molecular dynamics simulation. The three vibrational modes of a water molecule in the liquid phase are represented by the basis of two local OH stretching modes and an HOH bending mode. Since the characteristic frequencies of those vibrational modes are much higher than thermal energy at room temperature, a quantum-mechanical description is required for them. For simplicity, the bending mode is often ignored, and frozen to the average conformation of its ground state. In this case, the quantum-mechanical system is constituted by N local OH stretching modes (from $N/2$ water molecules) coupled to the classical bath. The adiabatic approximation is introduced for the quickly-moving quantum-mechanical modes and the slowly-moving classical bath, so that the Hamiltonian of the quantum-mechanical system depends parametrically on the bath coordinates. In this case, it is given by

$$H = \sum_{i=1}^{N} h_i(X_i;q) + v(X_1,\cdot\cdot,X_N;q) \qquad (7)$$

where h_i and X_i are, respectively, the Hamiltonian and coordinate of local OH mode i, and q collectively represents the bath coordinates. $v(X_1,\cdot\cdot,X_N;q)$ is the coupling Hamiltonian between the quantum modes, in which intra- and inter-molecular (dipole–dipole interaction) pair-wise coupling mechanisms are considered. As shown, both h_i and v depend on the bath coordinates.

In order to implement the QM/CM approach, Auer and Skinner performed an MD simulation using the SPC/E water model to obtain the dynamics of the classical bath, with the vibrational coordinates being frozen to their equilibrium values (defined to be zero). Then, a series of bath conformations were selected. For each selected conformation, electronic structure (ES) calculations using density functional theory were performed by varying the coordinate X_i of an arbitrarily chosen single mode i, while the other coordinates remain frozen. For computational efficiency, a cluster (whose average size was 9.25) of explicit waters around the mode was included in the ES calculations, and the remaining waters (within a spherical cutoff) were treated as point charges. In this way, the one-dimensional potential energy curve for the mode was constructed, resulting in the vibrational Hamiltonian of the mode, h_i. The two lowest eigenstates of the Hamiltonian along with their eigenvalues, from

$$\begin{aligned} h_i|0_i\rangle &= \varepsilon_i^0|0_i\rangle \\ h_i|1_i\rangle &= (\varepsilon_i^0 + \hbar\omega_i)|1_i\rangle \end{aligned} \qquad (8)$$

are calculated by using a discrete variable representation.[46]

These ES calculations on clusters are time consuming, and so it is not possible to perform them more than a few thousand times, whereas the spectroscopic calculations require well over a million simulation time steps, and hence configurations. One way to parameterize the bath dependence of the local frequency ω_i is to replace its dependence on the full set of bath coordinates, by its dependence on a single collective coordinate (which is a function of all bath coordinates). A convenient and useful collective coordinate is the electric field along O–H bond i, evaluated at the hydrogen atom.[38] A fit of the cluster frequencies (from ES calculations) to this electric field leads to a simple quadratic map.[26] Similarly, other quantities for the local mode such as the dipole derivative ($\mu_i' i \equiv |d\vec{\mu}/dX_i|_{\{X\}=0}$), and the transition distance ($x_i \equiv \langle 1_i|X_i|0_i\rangle$), have been mapped to the electric field.[26,38] Finally, the intramolecular and intermolecular coupling matrix elements, ω_{ij} (see below), have been parameterized, within the harmonic approximation, in terms of the field (and/or local frequencies).[36] Those relationships are presented in Table 1. By calculating the electric fields along the MD trajectory and using the mapping relationships, we can obtain trajectories of the local properties that are needed for the line shape calculations.

Table 1 Relationships for the transition frequency, ω_i, transition distance, x_i, dipole derivative, μ_i', intramolecular coupling frequency, $\omega_{ij}^{\text{intra}}$, and transition momentum, p_i, in terms of the electric field, E_i, or the transition frequency. The frequencies are in wave numbers and all other quantities are in atomic units. Intermolecular dipole–dipole coupling frequencies are calculated, within the harmonic approximation with respect to the vibrational coordinates, by the transition dipoles and distances displayed in the table (see ref. 36)

Property	Relationship
ω_i	$3762-5060E_i-86225E_i^2$
x_i	$0.1934-1.75\times10^{-5}\omega_i$
μ_i'	$0.1333 + 14.17E_i$
$\omega_{ij}^{\text{intra}}$	$\{-1789 + 23\,852(E_i + E_j)\}x_ix_j - 1.966p_ip_j$
p_i	$1.611 + 5.893\times10^{-4}\omega_i$

For the purpose of these calculations, the ground and singly-excited manifolds of vibrational modes are constructed by a direct product of the local eigenstates of h_i: $|0\rangle = |0_1\rangle\cdot\cdot|0_N\rangle$ and $|i\rangle = |0_1\rangle\cdot\cdot|1_i\rangle\cdot\cdot|0_N\rangle$ where $|0\rangle$ represents that all OH modes are in their ground states and $|i\rangle$ represents that the mode i is in its excited state and all the others are in their ground states. We ignore the coupling between the ground and singly-excited manifold states. With the many-mode basis representation, the Hamiltonian (7) can be written as

$$H = \sum_{i=1}^{N} |i\rangle\langle i|\hbar\omega_i + \sum_{i=1}^{N}\sum_{\substack{j=1\\ j\neq i}}^{N} |i\rangle\langle j|\hbar\omega_{ij} \qquad (9)$$

where $\hbar\omega_{ij} = \langle i|v|j\rangle$ for $i\neq j$ is the coupling matrix element between the states $|i\rangle$ and $|j\rangle$. We have subsumed a term, $\sum_{i=1}^{N}\varepsilon_i^0$, into the bath Hamiltonian.

Writing the time-correlation function in terms of the many-body states, and expanding the dipole operator with respect to the vibrational coordinates, eqn (2) becomes[36,43]

$$\phi_{IR}(T) = \frac{1}{3}\sum_{i,j=1}^{N}\langle \vec{m}_i(t)\cdot F_{ij}(t)\vec{m}_j(0)\rangle \qquad (10)$$

where

$$\vec{m}_i \equiv \mu_i' x_i \hat{u}_i \qquad (11)$$

is the transition dipole vector of OH bond i, whose unit vector is denoted by $\hat{u}_i$. $\vec{m}_i$ depends only on bath variables, and so it is explicitly time-dependent. $F(t)$ satisfies the kinetic equation

$$\frac{\mathrm{d}}{\mathrm{d}t}F(t) = -i\kappa(t)F(t) \qquad (12)$$

subject to the initial condition that $F_{ij}(0) = \delta_{ij}$, and with

$$\kappa_{ij}(t) = \omega_i(t)\delta_{ij} + \omega_{ij}(t)(1-\delta_{ij}) \quad (13)$$

where $\omega_i(t)$ and $\omega_{ij}(t)$ are the diagonal and off-diagonal fluctuating frequencies. The three time-dependent quantities, transition dipole $\vec{m}_i(t)$, transition frequency $\omega_i(t)$, and coupling frequency $\omega_{ij}(t)$, are obtained, by using the mapping relations, from the MD trajectory.

Similarly, the time-correlation functions of the isotropic and anisotropic polarizabilities that are needed to calculate the Raman line shapes are written, respectively, as

$$\Delta_{\mathrm{iso}}(t) = \sum_{i,j=1}^{N} \langle a_i(t) F_{ij}(t) a_j(0) \rangle \quad (14)$$

$$\Delta_{\mathrm{aniso}}(t) = \sum_{i,j=1}^{N} \langle Tr(\underline{\underline{b_i}}(t) \cdot F_{ij}(t) \underline{\underline{b_j}}(0)) \rangle \quad (15)$$

where

$$a_i \equiv \bar{\alpha}'_i x_i \quad (16)$$

$$\underline{\underline{b_i}} \equiv \underline{\underline{\beta}}'_i x_i \quad (17)$$

are, respectively, the isotropic and anisotropic transition polarizabilities of OH bond i. The bond polarizability model is employed to calculate the transition polarizability. In this model, the polarizability of a chemical bond is assumed to be cylindrically symmetric regardless of its environment, and the isotropic and anisotropic bond polarizability derivatives for OH bond i are given, respectively, by[47]

$$\bar{\alpha}'_i = \frac{1}{3}(\alpha'_{\parallel} + 2\alpha'_{\perp}) \quad (18)$$

$$\underline{\underline{\beta}}'_i = (\alpha'_{\parallel} - \alpha'_{\perp})\left(\hat{u}_i \otimes \hat{u}_i - \frac{1}{3}\underline{\underline{I}}\right) \quad (19)$$

where $\alpha'_{\parallel}$ and $\alpha'_{\perp}$ are, respectively, the parallel and perpendicular bond-polarizability derivatives, with the relation $\alpha'_{\parallel} = 5.6\alpha'_{\perp}$.[48] The isotropic bond polarizability derivative has been theoretically shown to be almost independent of bath coordinates in water,[49] but a similar bath-independence of the anisotropic bond polarizability derivative is yet to be confirmed.

IV. Results and discussion

Theoretical line shapes are calculated from the response functions, eqn (10) and (4)–(6) along with the time-correlation functions, eqn (14) and (15). The same MD method as in ref. 36, with the same number (128) of molecules, was employed to obtain the trajectories of various local properties at 300 K. $F_{ij}(t)$ in those time-correlation functions is obtained by numerically solving eqn (12). The IMSL routine IVMRK, which uses Runge–Kutta pairs of various orders, was employed to solve this differential equation, which, when averaged over 1000 different starting points, required approximately 0.5 CPU hour on Intel Xeon processor. We treat vibrational relaxation phenomenologically by multiplying the response functions by an exponential function

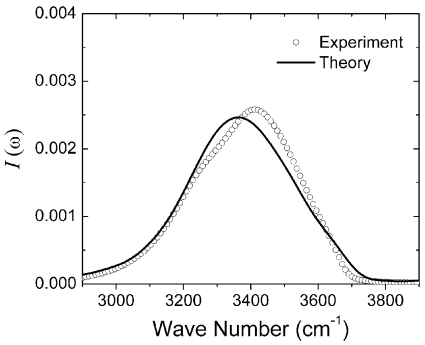

Fig. 1 Theoretical and experimental (ref. 52) IR line shapes for liquid water. Each line shape is normalized by area.

$\exp(-t/2T_1)$, with a lifetime $T_1 = 700$ fs.[50,51] Even though the experimental estimates for the lifetime of the OH stretching band range from 200[8,16] to 750 fs,[50] those differences do not make a significant change in the IR and Raman line shapes of water, which are all much broader than the inverse lifetime.

The theoretical IR absorption line shape is compared with the experimental spectrum[52] in Fig. 1. The theoretical line shape agrees very well with the experimental spectrum. In particular, the agreement for the full width at half maximum (FWHM) and the behavior of the red side of the line is excellent. With no adjustable parameters, it is highly encouraging for the theory to reproduce the experimental spectrum so well. However, the theory still fails in the predictions of the accurate location of the main peak at around 3400 cm^{-1} and the rapid decrease in the intensity at the blue side of spectrum. An improved water model for the MD simulation and/or better mapping models for frequency and transition dipoles may be helpful in removing such disagreements. We also note that this theoretical result is very similar to our previous result[36] using the time-averaging approximation,[43] differing only on the red side of the line. Thus the time-averaging approach provides a very good approximation to the exact result, although the small change on the red side of the line puts the exact result in better agreement with experiment.

With the success in reproduction of the experimental IR spectrum, we can now interpret the line shape. We start our discussion by noting the processes described in the time-domain expression for the line shape, eqn (10). A site j interacts with light *via* the transition dipole $\vec{m}_j$ and is excited at time zero. The excitation energy may stay at the site j or transfer to another site i. At a later time t, the probability amplitude for the excitation energy to be found at a site i is $F_{ij}(t)$, and the site i may be de-excited to its ground state by interaction with light *via* the transition dipole $\vec{m}_i(t)$. The de-excitation rate is proportional to the Franck–Condon (FC) overlap between the ground and excited states of the site (contained in $F_{ij}(t)$). The three consecutive steps of excitation, propagation, and de-excitation, collectively influence the line shape. Among them, the excitation and de-excitation processes are influenced by the statistics and fluctuations of transition dipoles, while the propagation is influenced by static and dynamic fluctuations of the transition energies (dephasing), and inter-site excitation energy transfer dynamics. These processes should presumably be correlated with each other *via* molecular motions.

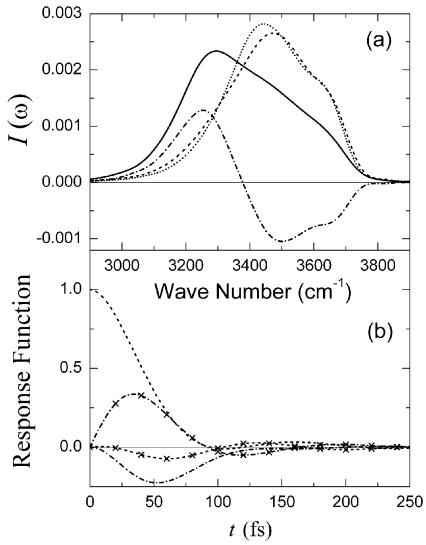

Fig. 2 IR line shape and response functions, but with a hypothetical homogeneous field-matter interaction ($\vec{m}_i = 1$). (a) Theoretical line shapes for uncoupled OH modes (dotted line), fully coupled water (solid line), and Fourier transforms of the diagonal (dashed line) and off-diagonal (dash-dotted line) response functions. (b) Real and imaginary (with cross symbols) parts of the diagonal (dashed line) and off-diagonal (dash-dotted line) response functions (normalized by the initial value of the response function). For ease of visualization, the response functions are multiplied by a phase factor $e^{i\omega_0 t}$, where $\omega_0 = 3460\ \mathrm{cm}^{-1}$ is a reference frequency.

First, in order to emphasize the effects of the propagation dynamics, we consider the hypothetical case that $\vec{m}_i(t)$ in eqn (10) is independent of i and constant in time, so that the line shape is determined solely by the ensemble average of the excitation propagation dynamics. We note that the response function for the isotropic Raman line shape (6) is such a case (with the exception of the very weak bath dependence of x_i). The assumption, however, is not applied to the transition dipoles in the intermolecular dipole–dipole coupling terms governing the energy transfer dynamics. Fig. 2a shows the theoretical line shape of such hypothetical water (solid line). The theoretical line shape when the intra- and intermolecular couplings are turned off (dotted line) is also displayed for comparison. The OH bonds of water are stretched by hydrogen bonds with other neighboring water molecules, and consequently the anharmonicity of the bonds increases. As a result, the frequencies of the hydrogen-bonded OH stretching modes are red-shifted.[19,20,24,25] The bimodal behavior in the line shape of uncoupled OH modes displayed in Fig. 2a by the dotted line demonstrates the inhomogeneous distribution of hydrogen-bonded and non-hydrogen-bonded OH stretching modes. The shoulder at around 3650 cm^{-1} arises from the OH modes that are not involved in hydrogen bonds, and the main peak located at around 3430 cm^{-1} results from the OH modes whose frequencies are red-shifted by hydrogen bonds. In addition, the OH frequency modulation due to intermolecular oscillations of the hydrogen bonds with a frequency of 180 cm^{-1} [53] (corresponding to an approximate period of less than 200 fs[11]) may lead to some contribution to the shoulder of the line shape. The spectral change caused by molecular couplings (solid line in Fig. 2a) is quite drastic. The most noticeable impact is the large red-shift ($\sim$150 cm^{-1}) in the peak position (which can be called an excitonic shift). The spectral change implies that the local excitation energies absorbed from light are *coherently* transferred to other sites within the time scale of vibrational dephasing (inverse line width, $\sim$100 fs in this case). This is consistent with the recent observations in polarization-sensitive pump–probe experiments.[13,16]

The effect of coherent energy transfer on the line shape can be understood most easily in the time domain. The line shape is the Fourier transform of the response function, which can be written as a sum of diagonal and off-diagonal terms, $\phi_{\mathrm{IR,\ diag}}(t) \sim \left\langle \sum_{j=1}^{N} F_{jj}(t) \right\rangle$ and $\phi_{\mathrm{IR,\ off\ diag}}(t) \sim \left\langle \sum_{i\neq j=1}^{N} F_{ij}(t) \right\rangle$. Apart from the decay by dephasing, the diagonal and off-diagonal terms also involve population transfer dynamics, resulting in the population at time t at the creation sites and at other sites, respectively. If molecular couplings are so weak that the excitation energy transfers more slowly than dephasing occurs, the off-diagonal response function becomes vanishingly small. Thus, if the off-diagonal response function is non-vanishing, excitation energy must transfer *coherently*. Therefore the transient behavior of the *off-diagonal* response function should exhibit distinctly the effects of molecular coupling. We plot the real and imaginary parts of the two response functions in Fig. 2b. The real part of $\phi_{\mathrm{IR,diag}}(t)$, represented by the dashed line, decays from its initial value mostly by dephasing, but additionally by population transfer through molecular coupling. Therefore, the line shape from this diagonal response function should be similar to that of uncoupled chromophores, but with additional broadening due to population transfer. On the other hand, when coherent population transfer occurs within the dephasing time, $\phi_{\mathrm{IR,off\text{-}diag}}(t)$ should grow in magnitude from zero with a rate proportional to the population transfer rate and then decay by dephasing. The transient rise of $\phi_{\mathrm{IR,off\text{-}diag}}(t)$ displayed in Fig. 2b illustrates that for the present system this is the case. Thus, the three noticeable features in the temporal behavior of the response functions displayed in Fig. 2b are: (1) an overall decay in about 100 fs (due to dephasing); (2) an oscillatory behavior with a period of about 150 fs (phase interference arising from the bimodal distribution of OH frequencies and, additionally, from the hydrogen-bond oscillation discussed in Fig. 2a); and (3) an initial rise in the amplitude of $\phi_{\mathrm{IR,off\text{-}diag}}(t)$ starting from zero (due to coherent energy transfer). The first two features appear in both the diagonal and off-diagonal response functions, and they are responsible, respectively, for dephasing-induced broadening and the shoulder located at 3650 cm^{-1} in the line shapes. The third feature in the off-diagonal response function is a unique characteristic arising from coherent energy transfer.

Now we transform the diagonal and off-diagonal response functions to the frequency domain, which are shown as the dashed and dash-dotted lines, respectively, in Fig. 2a. The solid line is, of course, the sum of these two lines. Thus we see, strikingly, that the effect of coherent energy transfer (dash-dotted line), is to diminish the intensity at around 3500 cm^{-1},

and enhance the intensity, dramatically, at about 3250 cm^{-1}, in fact creating the main peak in the theoretical spectrum. This peak is manifest to a lesser (in IR, as shown in Fig. 1) or greater (in polarized Raman, as shown below) extent in the different spectroscopies. Therefore, the appearance of the new band in the theoretical line shapes must be a strong signature of coherent energy transfer, even though the amplitude of the band may vary with the type of experiments, as discussed below. Thus, as Auer and Skinner[36] suggested, it is very likely that the shoulder at the red side of the experimental absorption spectrum is caused by the presence of coherent excitation energy transfer. We note that the off-diagonal response function produces substantial amplitudes over the whole range of frequencies. This implies that very rapid energy transfer is going on over essentially all the OH modes regardless of their local environments, although their mechanisms may be different depending on the frequencies of the involved chromophores (see below).

In addition to the red-shift of peak positions, we can see that the line shape in Fig. 2a becomes broader as a result of molecular couplings. This is in contrast with the exchange narrowing often found in electronic spectroscopies of well-ordered strongly-coupled molecular aggregates.[54] Strong coupling induces fast energy transfer and consequently make an effective motional (exchange) narrowing of inhomogeneous broadening. The opposite tendency observed here in the vibrational line shape of water is due to the strong non-Condon effects associated with dipole–dipole couplings. The Skinner group[49,55] showed that transition dipoles of OH stretch modes depend strongly on their hydrogen-bonding environments, and this was experimentally confirmed by a comparison of IR and Raman spectra.[2] The transition dipoles of non-hydrogen-bonded OH stretch modes (spectrally located in the high-frequency region) are significantly smaller than those of hydrogen-bonded OH modes (spectrally located in the low-frequency region). Therefore, the intermolecular dipole–dipole couplings inducing the excitonic shift are strong for hydrogen-bonded water molecules in the low-frequency region, while they are a bit weaker for non-hydrogen bonded water molecules in the high-frequency region. Thus, the red spectral region is more red-shifted than is the blue spectral region. As a result, the overall line shape gets wider in Fig. 2a due to such inhomogeneous molecular couplings caused by the strong non-Condon transition dipoles reflected in the molecular couplings.

Next we interpret the theoretical IR line shape for real, not hypothetical, water (where the magnitudes and directions of the transition dipoles are properly taken into account), within the same time-domain picture. In Fig. 3a we show the theoretical IR line shape (solid line), its decomposition into two terms from the diagonal (dashed line) and off-diagonal (dash-dotted line) response functions. The dotted line shows the theoretical IR line shape when the chromophores are not coupled. First we compare the line shape for the uncoupled OH modes with that in Fig. 2a. Due to the weak transition dipoles of the OH modes spectrally located at around 3650 cm^{-1}, the light-induced transition amplitude at that frequency region is significantly reduced in Fig. 3a as we take into account the dependence of transition dipoles on the bath coordinates.

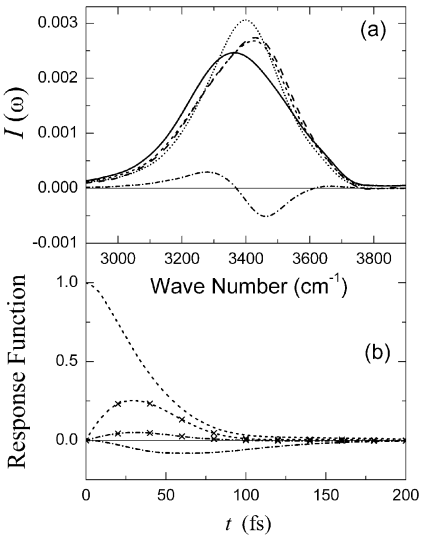

Fig. 3 Same as Fig. 2, except here the results (with the exception of the long dashed line) are for real water. In (a), the long dashed line is for a second hypothetical water where the transition dipoles in the field–matter interaction are randomly oriented.

Namely, the non-hydrogen-bonded OH modes make weaker light-induced transitions than hydrogen-bonded OH modes do, as discussed in ref. 2 and 55.

The effects of molecular couplings on the line shape in Fig. 3a appear to be not as great as in Fig. 2a. Comparing the line shapes of uncoupled OH and water in Fig. 3a, we can see the line shape of neat water is excitonically red-shifted only by about 30 cm^{-1}, which is much smaller than the 150 cm^{-1} in Fig. 2a, and the overall width is only mildly broadened by molecular couplings. Experimental spectra in the OH stretching region actually exhibit a similarly small difference between HOD in D_2O and water.[14,52] Without a careful analysis, those experimental and theoretical observations might mislead one to conclude that the extent of vibrational excitation energy transfer in water is small. However, the reduced impact of molecular couplings to line shape in this case is a result of additional dephasing due to the disordered orientation of transition dipoles.

To explore this idea further, we consider the diagonal and off-diagonal response functions for the line shape, $\phi_{\mathrm{IR,diag}}(t) \sim \left\langle \sum_{j=1}^{N} \vec{m}_j(t) \cdot F_{jj}(t) \vec{m}_j \right\rangle$ and $\phi_{\mathrm{IR,off\text{-}diag}}(t) \sim \left\langle \sum_{i \neq j=1}^{N} \vec{m}_i(t) \cdot F_{ij}(t) \vec{m}_j \right\rangle$, which now include the statistics and fluctuations of transition dipoles as well as the quantum dynamics of excited vibrational states. The temporal profiles of the two response functions are displayed in Fig. 3b. The diagonal response function (dashed lines) is essentially similar to that in Fig. 2b, except for the opposite sign of the imaginary part (with cross symbols) at early times (which is because the red side of the frequency distribution has more optical activity due to the non-Condon effects). However, in comparison with that in Fig. 2b, the amplitude of the off-diagonal response function (dash-dotted lines) is much smaller. The off-diagonal response function may be understood as an *effective* rotational time-correlation function of transition dipoles evolving along

with excitation energy moving around. Therefore, even though local excitation energies are coherently transferred (as described in $F_{ij}(t)$), the transition dipoles (orientations) of energy acceptors are not perfectly correlated to those of energy donors and the coherency of the excited energy acceptors is not manifested due to the randomized orientations of transition dipoles. As a result, the amplitude of the off-diagonal response function is greatly reduced compared with that in Fig. 2b, and the spectral change due to molecular couplings appears weak in Fig. 3a, since the coherence is washed out by "rotations" of transition dipoles. For example, if the transition dipoles in the field-matter interaction terms are completely random in orientation (long-dashed line in Fig. 3a), the line shape is very similar to that from the diagonal response function alone, showing that the random distribution of orientation almost completely obscures the extent of coherent energy transfer. Therefore, the theoretical IR line shape, seemingly not so different from that for uncoupled OH modes (Fig. 3a), actually results from a delicate balance between the effects of coherent energy transfer and disorder in the orientation of transition dipoles. The small red shift from the long-dashed to the solid line shapes, though, reflects a certain degree of remaining structural order of liquid water.

In this context, it is now especially interesting to consider the Raman line shapes. The time-correlation functions of the isotropic and anisotropic polarizabilities defined by eqn (14) and (15) are responsible for the Raman spectroscopies. For the time being, let us simply ignore the bath dependence of the transition distance x_i in the time-correlation functions. Then, within the bond-polarizability model, the two time-correlation functions are reduced to

$$\Delta_{\mathrm{iso}}(t) \sim \sum_{i,j=1}^{N} \langle F_{ij}(t) \rangle \tag{20}$$

$$\Delta_{\mathrm{aniso}}(t) \sim \sum_{i,j=1}^{N} \left\langle Tr\left(\left(\hat{u}_i(t) \otimes \hat{u}_i(t) - \frac{1}{3}\underline{\underline{I}} \right) \cdot F_{ij}(t) \left(\hat{u}_j(0) \otimes \hat{u}_j(0) - \frac{1}{3}\underline{\underline{I}} \right) \right) \right\rangle. \tag{21}$$

$\Delta_{\mathrm{iso}}(t)$ fully retrieves the effects of coherent energy transfer contained in $F_{ij}(t)$, but $\Delta_{\mathrm{aniso}}(t)$, being dressed by the "effective rotation" of the OH bonds resulting from energy transfer as well as by the molecular rotations, does not. Therefore the characteristic band of coherent energy transfer is expected to appear in the isotropic and VV Raman line shapes, while it should be smeared out by the effective pseudo-random rotations in the VH Raman line shape. Fig. 4 shows the theoretical and experimental Raman line shapes. As with our previous time-averaging approximation results, agreement between theory and experiment is rather good. And as expected, the characteristic band of coherent energy transfer completely disappears in the theoretical and experimental VH Raman line shapes, while it is clearly apparent in the VV Raman line shapes. Therefore the distinct behavior in the red side of the VV and VH Raman spectra related to so-called non-coincidence effects,[56] is caused by the different nature of the field-matter interactions (isotropic *vs.* anisotropic

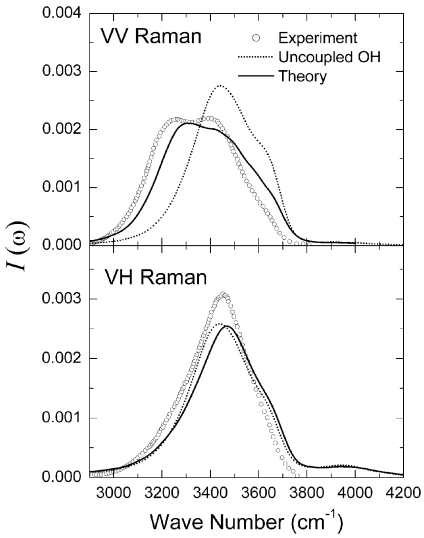

Fig. 4 Theoretical and experimental (ref. 40) Raman line shapes. The theoretical line shapes for uncoupled OH modes (dotted lines) are also displayed for comparison. Each line shape is normalized by area.

polarizabilities). The bands at 3250 cm^{-1} in the experimental IR absorption and VV Raman spectra, albeit with different strengths, have the same origin: coherent vibrational energy transfer.

Other notable features in the VH Raman line shape are the weak shoulder at 3650 cm^{-1} from the uncoupled OH bonds, and the unique appearance of the broad bands at the far blue side from 3800 to 4200 cm^{-1}. Those features, which range continuously from zero up to about 500 cm^{-1}, arise from the inertial ($\sim$100 fs) contributions to librational and hindered translational motion of OH bonds,[13,16,30] which appear through the time dependence of the anisotropic components of the polarizability tensor. This broad band does not appear in Fig. 2a and 4a. This suggests that those particular modes make little contribution to frequency fluctuations. The same conclusion has been arrived at by a polarization-sensitive IR pump–probe experiment observing the rapid libration dynamics of HOD in D_2O with a 50 fs time constant[14,57] and by theoretical calculations.[24,58] Absence of the bands in Fig. 3a, in which the rotations and non-Condon effects are accounted for, also implies that the bands are mainly associated with the non-hydrogen bonded OH bonds with weak transition amplitudes. Theoretical and experimental studies[22,25,30,37] have indeed shown that these molecules show a faster reorientation decay due to librations. This broad band on the blue side of the depolarized Raman spectra has in fact been seen experimentally.[3]

Fig. 5 compares the theoretical line shapes for the four different types of experiments, which show, to differing extents, signatures of coherent energy transfer. The isotropic Raman line shape, which is determined by the isotropic polarizability, exhibits the largest amplitude for the characteristic band, followed by the VV Raman, IR absorption, and VH Raman line shapes.

Before we conclude, we wish to make two more points, not directly related to the main thrust of this paper. The spectral change induced by molecular couplings may be understood

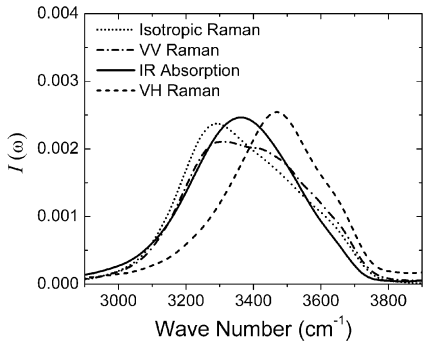

Fig. 5 Theoretical line shapes for four different experiments, as indicated in the legend.

also in the delocalized eigenstate picture. Delicate quantum interference effects of local excited states produce new excited states (eigenstates) delocalized over many chromophores, each with its own transition amplitude. If the bath is static (the inhomogeneous limit), the spectral density of those eigenstates are given by

$$I_{in}(\omega) \sim \sum_{k=1}^{N} \langle d_k^2 \delta(\omega - \lambda_k) \rangle \qquad (22)$$

where d_k and λ_k are the transition dipole and eigen-frequency of a delocalized eigenstate k. Auer and Skinner[36] directly diagonalized an ensemble of instantaneous vibrational Hamiltonians constructed from a trajectory of their MD simulation. It was found that the delocalization, defined by the inverse participation ratio, extends over approximately ten molecules. Thus, even though the molecular couplings are not so great as to make the frequency distribution of eigenstates different from that of uncoupled chromophores, they are great enough to make the eigenstates spatially extended, and consequently their *spectral* distribution is altered substantially from that of locally excited states. Due to the compact structure of water, and long-ranged dipole–dipole interactions, each vibrational mode selects optimally its isoenergetic coupling partners from the chromophores largely disordered in energy, so that efficient energy transfer is readily achievable even by small couplings. The excitonic red-shift is similar to the case of J-aggregates, where parallel transition dipoles lead to negative coupling elements.

This analysis implicitly assumes that the static picture is correct "enough". In fact, time-dependent transition frequency and coupling fluctuations cause the instantaneous eigenstates to evolve in time. If this is sufficiently fast, it will cause motional narrowing in the spectrum. To provide some quantitative information about the adequacy of this static approximation, in Fig. 6 we present a direct comparison of the spectral density in (22), with the theoretical IR line shape (which includes all dynamical effects). The top panel shows results for hypothetical water (discussed earlier), and the bottom panel shows results for real water. This comparison for hypothetical water shows a modest dynamical effect, resulting in a narrowing of the line shape, and enhancement of the characteristic molecular coupling band. The result for real water shows a smaller effect. Spectral densities and theoretical line shapes for VV and VH Raman spectra are

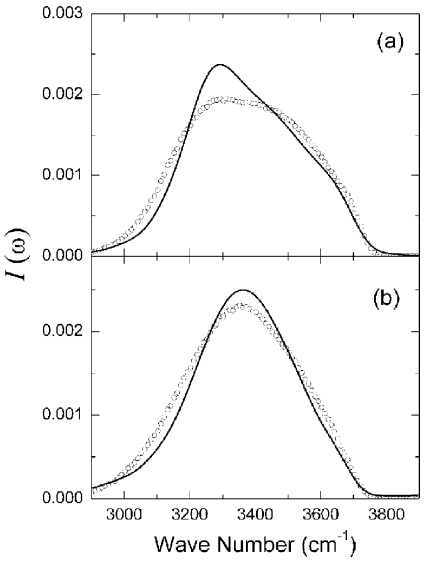

Fig. 6 Theoretical IR absorption line shapes (solid line) and spectral densities (open circles). (a) hypothetical water. (b) real water.

shown in Fig. 7. Here the dynamical effects of motional narrowing are more significant than for the IR spectrum, but still rather modest. Our conclusion is that because the effects of dynamical fluctuations are quite small, our original analysis based on the static limit is qualitatively correct.

A second point has to do with the relative effects of intra- and intermolecular coupling in causing coherent energy transfer (or producing eigenstate delocalization). Fig. 8 displays the theoretical line shapes for the four cases of uncoupled chromophores, intramolecular coupling only, intermolecular coupling only, and fully coupled chromophores, for hypothetical water (upper panel), and for the IR spectrum (lower panel). For both coupling mechanisms, we can see excitonic red-shifts ($\sim$25 cm^{-1} from the intramolecular couplings and $\sim$125 cm^{-1} from the intermolecular couplings). Interestingly,

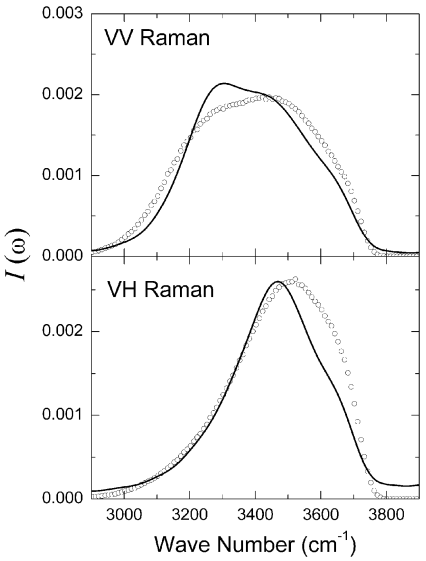

Fig. 7 Theoretical Raman line shapes (solid line) and spectral densities (open circles).

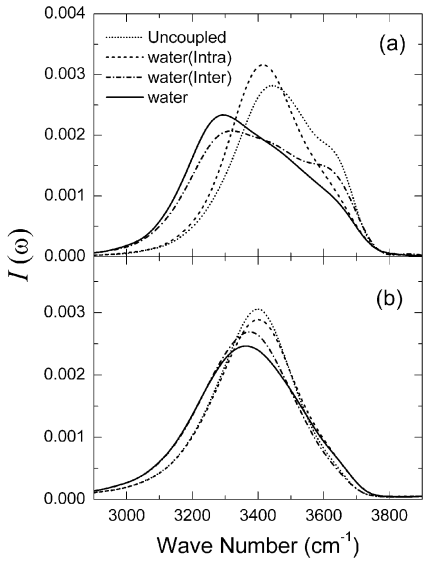

Fig. 8 Theoretical line shapes for four cases: Uncoupled OH (dotted line), water with intramolecular couplings only (dashed line), water with intermolecular couplings only (dash-dotted line), water with full couplings (solid line). (a) Hypothetical water. (b) IR line shape for real water.

the excitonic shifts from each contribution are additive, giving the excitonic shift (150 cm^{-1}) of fully-coupled water. Noting that the average energies of intra- and intermolecular pair-wise couplings are similar in magnitude (~ -27 cm^{-1}, see ref. 36), the characteristic band associated with the intersite couplings must result from energy transfer occurring collectively *over many chromophores* (rather than occurring in one step).

It is interesting to note, from Fig. 8a, that the deviations of fully-coupled water, from uncoupled water, are due on the red side almost entirely to the intermolecular interactions, and on the blue side almost entirely to intramolecular coupling. In fact, this is easy to understand, since through the non-Condon effects, the intermolecular coupling is much larger on the red side (than on the blue), and through the decrease of the intramolecular coupling with increased hydrogen bonding,[36] the intramolecular coupling is larger on the blue side. This same scenario prevails, but more weakly, in the lower panel (for the IR spectrum).

V. Conclusions

Using a mixed QM/CM approach recently developed by Auer and Skinner, we calculated the IR and Raman line shapes of neat water in the spectral range of the OH stretching frequency. Within the model, all dynamical effects of transition frequency, dipole, polarizability, and vibrational coupling fluctuations have been treated exactly, improving on our earlier results,[36] which involved the time-averaging approximation. Excellent agreement between the theoretical and experimental line shapes has been achieved without introducing any adjustable parameters.

By separating the response function into diagonal and off-diagonal contributions, we provide a time-domain interpretation of the experimental results, and especially of the origin of the low-frequency band at about 3250 cm^{-1}, which is complementary to the frequency-domain interpretation provided earlier.[36] This time-domain interpretation makes it abundantly clear that the origin of the band is coherent vibrational energy transfer. Note that the same intersite couplings that lead to this coherent energy transfer, produce delocalized eigenstates (which is the origin of this band in the frequency-domain picture).

It is particularly interesting to understand how different experiments (IR, isotropic Raman, and depolarized Raman) manifest this collective band differently. We show explicitly that these differences arise from the scalar, vector, and tensor nature of the field-matter interactions, for isotropic Raman, IR, and depolarized Raman, respectively. In particular, the disorder in the vector and tensor interactions, inherent in the liquid, suppresses the appearance of the collective band in IR and depolarized Raman experiments. For example, then, it is misleading to conclude from the similarity of the IR spectrum for water and dilute HOD in D_2O, that the effects of vibrational coupling are small. In fact, they do not show up in the IR spectrum because of the delicate cancellation between coherent energy transfer and rotational disorder. To appreciate the full extent of coherent vibrational energy transfer in liquid water, one must consider IR *and* (isotropic and depolarized) Raman experiments. The isotropic Raman line shape, which shows no effect of rotational disorder, has the most pronounced collective band. This new time-domain analysis reinforces our view[36] that the symmetric and anti-symmetric normal mode basis is not particularly appropriate or useful for understanding the vibrational spectroscopy of liquid water, and that the features in the various spectra cannot be understood solely in terms of the local environments of individual molecules, but rather must reflect the effects of intra- and intermolecular vibrational coupling.

We anticipate that a similar time-domain analysis will be useful in interpreting theoretical results for other vibrational spectroscopy on water, such as the vibrational sum-frequency spectroscopy of the liquid/vapor interface,[27,59] and the 2DIR spectroscopy of bulk liquid water.[33,60]

Acknowledgements

We thank P. Pieniazek and B. M. Auer for generating and providing the MD trajectory. This work was supported by the Korea Research Foundation Grant funded by the Korean Government (MOEHRD, Basic Research Promotion Fund) (KRF-2008-314-C00166), and by the US NSF (CHE-0750307), DOE (DE-FG02-09ER16110), and the University of Wisconsin Foundation.

References

1 J. B. Brubach, A. Mermet, A. Filabozzi, A. Gerschel and P. Roy, *J. Chem. Phys.*, 2005, **122**, 184509.
2 J. J. Loparo, S. T. Roberts, R. A. Nicodemus and A. Tokmakoff, *Chem. Phys.*, 2007, **341**, 218–229.
3 W. F. Murphy and H. J. Bernstein, *J. Phys. Chem.*, 1972, **76**, 1147–1152.
4 J. R. Scherer, M. K. Go and S. Kint, *J. Phys. Chem.*, 1974, **78**, 1304–1313; J. L. Green, A. R. Lacey and M. G. Sceats, *J. Phys. Chem.*, 1986, **90**, 3958–3964; D. E. Hare and C. M. Sorensen,

J. Chem. Phys., 1992, **96**, 13–22; K. Winkler, J. Lindner and P. Vöhringer, *Phys. Chem. Chem. Phys.*, 2002, **4**, 2144–2155; M. Pastorczak, M. Kozanecki and J. Ulanski, *J. Phys. Chem. A*, 2008, **112**, 10705–10707.
5 D. M. Carey and G. M. Korenowski, *J. Chem. Phys.*, 1998, **108**, 2669–2675.
6 N. A. Chumaevskii and M. N. Rodnikova, *J. Mol. Liq.*, 2002, **96–97**, 31–43; J. D. Smith, C. D. Cappa, K. R. Wilson, R. C. Cohen, P. L. Geissler and R. J. Saykally, *Proc. Natl. Acad. Sci. U. S. A.*, 2005, **102**, 14171–14174.
7 S. Woutersen and H. J. Bakker, *Nature*, 1999, **402**, 507–509.
8 A. J. Lock and H. J. Bakker, *J. Chem. Phys.*, 2002, **117**, 1708–1713.
9 H. J. Bakker, A. J. Lock and D. Madsen, *Chem. Phys. Lett.*, 2004, **385**, 329–331; Z. Wang, A. Kakoulev, Y. Pang and D. D. Dlott, *J. Phys. Chem. A*, 2004, **108**, 9054–9063; J. C. Deàk, S. T. Rhea, L. K. Iwaki and D. D. Dlott, *J. Phys. Chem. A*, 2000, **104**, 4866–4875.
10 R. Laenen, C. Rauscher and A. Laubereau, *J. Phys. Chem. B*, 1998, **102**, 9304–9311; R. Laenen, C. Rauscher and A. Laubereau, *Phys. Rev. Lett.*, 1998, **80**, 2622–2625.
11 C. J. Fecko, J. D. Eaves, J. J. Loparo, A. Tokmakoff and P. L. Geissler, *Science*, 2003, **301**, 1698–1702.
12 J. B. Asbury, T. Steinel, C. Stromberg, S. A. Corcelli, C. P. Lawrence, J. L. Skinner and M. D. Fayer, *J. Phys. Chem. A*, 2004, **108**, 1107–1119; J. B. Asbury, T. Steinel, K. Kwak, S. A. Corcelli, C. P. Lawrence, J. L. Skinner and M. D. Fayer, *J. Chem. Phys.*, 2004, **121**, 12431–12446.
13 M. L. Cowan, B. D. Bruner, N. Huse, J. R. Dwyer, B. Chugh, E. T. J. Nibbering, T. Elsaesser and R. J. D. Miller, *Nature*, 2005, **434**, 199–202.
14 C. J. Fecko, J. J. Loparo, S. T. Roberts and A. Tokmakoff, *J. Chem. Phys.*, 2005, **122**, 054506.
15 J. D. Eaves, J. J. Loparo, C. J. Fecko, S. T. Roberts, A. Tokmakoff and P. L. Geissler, *Proc. Natl. Acad. Sci. U. S. A.*, 2005, **102**, 13019–13022.
16 D. Kraemer, M. L. Cowan, A. Paarmann, N. Huse, E. T. J. Nibbering, T. Elsaesser and R. J. D. Miller, *Proc. Natl. Acad. Sci. U. S. A.*, 2008, **105**, 437–442.
17 S. A. Rice, M. Bergren, A. C. Belch and G. Nielson, *J. Phys. Chem.*, 1983, **87**, 4295–4308.
18 I. Ohmine and S. Saito, *Acc. Chem. Res.*, 1999, **32**, 741–749; M. T. Sonoda, S. M. Vechi and M. S. Skaf, *Phys. Chem. Chem. Phys.*, 2005, **7**, 1176–1180; V. Buch, T. Tarbuck, G. L. Richmond, H. Groenzin, I. Li and M. J. Shultz, *J. Chem. Phys.*, 2007, **127**, 204710.
19 R. Rey, K. B. Moller and J. T. Hynes, *J. Phys. Chem. A*, 2002, **106**, 11993–11996.
20 K. B. Moller, R. Rey and J. T. Hynes, *J. Phys. Chem. A*, 2004, **108**, 1275–1289.
21 V. Buch, *J. Phys. Chem. B*, 2005, **109**, 17771–17774.
22 D. Laage and J. T. Hynes, *Science*, 2006, **311**, 832–835.
23 C. P. Lawrence and J. L. Skinner, *J. Chem. Phys.*, 2002, **117**, 8847–8854; W. Chen, M. Sharma, R. Resta, G. Galli and R. Car, *Phys. Rev. B: Condens. Matter Mater. Phys.*, 2008, **77**, 245144.
24 C. P. Lawrence and J. L. Skinner, *Chem. Phys. Lett.*, 2003, **369**, 472–477.
25 C. P. Lawrence and J. L. Skinner, *J. Chem. Phys.*, 2003, **118**, 264–272.
26 B. Auer, R. Kumar, J. R. Schmidt and J. L. Skinner, *Proc. Natl. Acad. Sci. U. S. A.*, 2007, **104**, 14215–14220.
27 B. M. Auer and J. L. Skinner, *J. Chem. Phys.*, 2008, **129**, 214705.
28 B. M. Auer and J. L. Skinner, *Chem. Phys. Lett.*, 2009, **470**, 13–20.
29 Y. L. A. Rezus and H. J. Bakker, *J. Chem. Phys.*, 2006, **125**, 144512.
30 D. E. Moilanen, E. E. Fenn, Y. S. Lin, J. L. Skinner, B. Bagchi and M. D. Fayer, *Proc. Natl. Acad. Sci. U. S. A.*, 2008, **105**, 5295–5300.
31 H. Torii, *J. Phys. Chem. A*, 2006, **110**, 9469–9477.
32 H. Torii, *J. Mol. Liq.*, 2007, **136**, 274–280; S. Habershon, G. S. Fanourgakis and D. E. Manolopoulos, *J. Chem. Phys.*, 2008, **129**, 074501.
33 A. Paarmann, T. Hayashi, S. Mukamel and R. J. D. Miller, *J. Chem. Phys.*, 2008, **128**, 191103.
34 T. l. C. Jansen and W. M. Ruszel, *J. Chem. Phys.*, 2008, **128**, 214501; C. Falvo, B. Pamieri and S. Mukamel, *J. Chem. Phys.*, 2009, **130**, 184501.
35 T. Hayashi, T. l. C. Jansen, W. Zhuang and S. Mukamel, *J. Phys. Chem. A*, 2005, **109**, 64–82.
36 B. M. Auer and J. L. Skinner, *J. Chem. Phys.*, 2008, **128**, 224511.
37 J. L. Skinner, B. Auer and Y. S. Lin, *Adv. Chem. Phys.*, 2009, **142**, 59–103.
38 S. A. Corcelli, C. P. Lawrence and J. L. Skinner, *J. Chem. Phys.*, 2004, **120**, 8107–8117.
39 H. J. C. Berendsen, J. R. Grigera and T. P. Straatsma, *J. Phys. Chem.*, 1987, **91**, 6269–6271.
40 G. E. Walrafen, M. S. Hokmabadi and W. H. Yang, *J. Chem. Phys.*, 1986, **85**, 6964–6969.
41 P. A. Giguere, *J. Chem. Phys.*, 1987, **87**, 4835–4839; G. E. Walrafen and Y. C. Chu, *J. Phys. Chem.*, 1995, **99**, 11225–11229; R. H. Li, Z. P. Jiang, F. G. Chen, H. W. Yang and Y. T. Guan, *J. Mol. Struct.*, 2004, **707**, 83–88; D. A. Schmidt and K. Miki, *J. Phys. Chem. A*, 2007, **111**, 10119–10122.
42 A. Sokolowska and Z. Kecki, *J. Raman Spectrosc.*, 1986, **17**, 29–33; Y. Tominaga, A. Fujiwara and Y. Amo, *Fluid Phase Equilib.*, 1998, **144**, 323–330.
43 B. M. Auer and J. L. Skinner, *J. Chem. Phys.*, 2007, **127**, 104105.
44 T. l. C. Jansen and J. Knoester, *J. Phys. Chem. B*, 2006, **110**, 22910–22916; R. D. Gorbunov, P. H. Nguyen, M. Kobus and G. Stock, *J. Chem. Phys.*, 2007, **126**, 054509.
45 D. A. McQuarrie, *Statistical Mechanics*, University Science Books, Sausalito, 2000.
46 D. J. Tannor, *Introduction to Quantum Mechanics: A Time-Dependent Perspective*, University Science Books, 2006.
47 A. C. Belch and S. A. Rice, *J. Chem. Phys.*, 1983, **78**, 4817–4823.
48 J. R. Scherer and R. G. Snyder, *J. Chem. Phys.*, 1977, **67**, 4794–4811; J. E. Bertie, B. F. Francis and J. R. Scherer, *J. Chem. Phys.*, 1980, **73**, 6352–6353.
49 S. A. Corcelli and J. L. Skinner, *J. Phys. Chem. A*, 2005, **109**, 6154–6165.
50 Z. H. Wang, A. Pakoulev, Y. Pang and D. D. Dlott, *Chem. Phys. Lett.*, 2003, **378**, 281–288; A. Pakoulev, Z. H. Wang and D. D. Dlott, *Chem. Phys. Lett.*, 2003, **371**, 594–600; A. Pakoulev, Z. H. Wang, Y. S. Pang and D. D. Dlott, *Chem. Phys. Lett.*, 2004, **385**, 332–335.
51 H. T. Dong and R. A. Wheeler, *Chem. Phys. Lett.*, 2005, **413**, 176–181.
52 J. E. Bertie and Z. Lan, *Appl. Spectrosc.*, 1996, **50**, 1047–1057.
53 G. E. Walrafen, M. R. Fisher, M. S. Hokmabadi and W. H. Yang, *J. Chem. Phys.*, 1986, **85**, 6970–6982.
54 P. B. Walczak, A. Eisfeld and J. S. Briggs, *J. Chem. Phys.*, 2008, **128**, 044505.
55 J. R. Schmidt, S. A. Corcelli and J. L. Skinner, *J. Chem. Phys.*, 2005, **123**, 044513.
56 P. Mirone and G. Fini, *J. Chem. Phys.*, 1979, **71**, 2241–2243; C. H. Wang and J. McHale, *J. Chem. Phys.*, 1980, **72**, 4039–4044; J. L. McHale, *J. Chem. Phys.*, 1981, **75**, 30–35; D. E. Logan, *Chem. Phys.*, 1986, **103**, 215–225; H. Torii and M. Tasumi, *J. Chem. Phys.*, 1993, **99**, 8459–8465; H. Torii, *Chem. Phys. Lett.*, 2000, **323**, 382–388.
57 J. J. Loparo, C. J. Fecko, J. D. Eaves, S. T. Roberts and A. Tokmakoff, *Phys. Rev. B: Condens. Matter Mater. Phys.*, 2004, **70**, 180201.
58 J. D. Eaves, A. Tokmakoff and P. L. Geissler, *J. Phys. Chem. A*, 2005, **109**, 9424–9436.
59 B. M. Auer and J. L. Skinner, *J. Phys. Chem. B*, 2009, **113**, 4125–4130.
60 A. Paarmann, T. Hayashi, S. Mukamel and R. J. D. Miller, *J. Chem. Phys.*, 2009, **130**, 204110.